COMPARISON OF THE PROFILE STRUCTURES OF ISOLATED AND RECONSTITUTED SARCOPLASMIC RETICULUM MEMBRANES

L. HERBETTE, A. SCARPA, AND J. K. BLASIE, *Departments of Chemistry and Biochemistry/Biophysics, University of Pennsylvania, Philadelphia, Pennsylvania 19104; Department of Biology, Brookhaven National Laboratory, Upton, New York 11973*

C. T. WANG, A. SAITO, AND S. FLEISCHER, *Department of Molecular Biology, Vanderbilt University, Nashville, Tennessee 37235*

ABSTRACT The profile structures of functional reconstituted sarcoplasmic reticulum (RSR) membranes were investigated as a function of the lipid/protein (L/P) ratio via x-ray diffraction studies of hydrated oriented multilayers of these membranes to a resolution of 10–15 Å, and neutron diffraction studies on these multilayers to lower resolutions. Our results at this stage of investigation indicate that reconstitution of SR with variable amounts of Ca^{2+} pump protein for L/P ratios >88 results in closed membraneous vesicles in which the Ca^{2+} pump protein is distributed asymmetrically in the membrane profile; a majority of the protein density is contained primarily in the extravesicular half of the membrane profile whereas a relatively lesser portion of the protein spans the hydrocarbon core of the RSR membranes. These RSR membranes are functionally similar and resemble isolated light sarcoplasmic reticulum in both profile structure and function at a comparable L/P ratio. Reconstitution with greater amounts of Ca^{2+} pump protein (e.g. L/P ~50–60) resulted in substantially less functional membranes with a dramatically thicker profile structure.

INTRODUCTION

Reconstituted sarcoplasmic reticulum (RSR) vesicles have been shown to be highly functional in terms of ATP-induced Ca^{2+} uptake with regard to isolated light sarcoplasmic reticulum (LSR) controls (1). The RSR membrane system has been well characterized with respect to the type of molecular species present, being composed essentially of the Ca^{2+} pump protein associated with the normal SR lipid mixture (2). The simple composition and function and the ability to alter the ratio of protein and lipid components in the membrane make this membrane system an ideal prospect for structural studies via x-ray and neutron diffraction.

Such structural studies are facilitated by utilizing hydrated oriented multilayers of the SR[1] membranes. The proper analysis of meridional lamellar x-ray and neutron diffraction data from such multilayers can provide the membrane's electron and neutron scattering density profiles. These profiles arise from a projection of the membrane structure along a direction

[1]SR will refer only to the highly purified sarcoplasmic reticulum prepared according to Meissner et al., (17); specifically, light, intermediate, and heavy sarcoplasmic reticulum, designated LSR, ISR, and HSR, respectively, will refer to the upper, intermediate, and lower fractions obtained from the isopycnic gradient (18).

parallel to the membrane plane onto an axis normal to that plane, and are therefore due to the average distribution of membrane molecular components projected onto this profile axis (3). Hence, a considerable amount of information can be obtained from such studies regarding the distribution and sub-structure of the membrane's molecular components within the membrane profile structure if the membrane's composition is simple and if the ratio or scattering contrast of its components can be varied (4–10).

We have determined the electron density profiles of the isolated LSR membrane and the RSR membrane for several lipid-to-protein (L/P) ratios to a resolution of ~10–15 Å. The low resolution (~40 Å) water profiles of the isolated LSR membrane and the RSR membrane for the same L/P ratios were obtained directly by analysis of the lamellar neutron diffraction and found to be in agreement with the electron density profiles. Inspection of these various profiles provided qualitative information on the distribution and substructure of Ca^{2+} pump protein and lipid within the RSR and LSR membrane profile structures. The derived LSR and RSR membrane electron density profiles are generally consistent with the electron microscope images of these membrane profiles observed in cross sections of hydrated oriented membrane multilayers prepared in the same manner as those used for x-ray and neutron experimentation (11–13).

Oriented membrane multilayers of isolated LSR under the conditions of the diffraction experiments have been shown to maintain up to 80% of their maximal functional activity with respect to ATP-induced Ca^{2+} accumulation, as measured in redispersions and directly in partially dehydrated multilayers (14). The structural results for the isolated and reconstituted SR membrane systems reported here therefore pertain to a highly functional state of these membranes and may be directly correlated with the ATP-induced Ca^{2+} accumulation and ATPase activity measurements described in the previous paper (1).

METHODS

Preparation of Reconstituted SR Vesicles

RSR vesicles with different L/P ratios were prepared as described (1, 2) and suspended in a solution containing 300 mM sucrose, 100 mM KCl, 1 mM Hepes, pH 7.1. Samples were quickly frozen and stored in liquid nitrogen until use. Protein concentrations were determined by the method of Lowry et al. (15) using bovine serum albumin as a standard. Lipid phosphorous was estimated from a determination of the total phosphorous content according to the method of Meissner and Fleischer (16). The L/P ratio is expressed as mole phospholipid per mole protein (mole PL/mole prot) throughout this paper. LSR vesicles were isolated and purified as described (17, 18).

X-ray Diffraction Studies

PREPARATION OF HYDRATED ORIENTED MEMBRANE MULTILAYERS Isolated LSR and RSR samples (0.5 mg protein) were diluted with 100mM KCl, 10 mM $MgCl_2$, 2 mM Tris Maleate, pH 7.0 (medium 1), and oriented membrane multilayers were prepared for x-ray diffraction studies as described (14). The resulting oriented multilayer specimens were partially dehydrated at 93% relative humidity (RH) at 5°C. Oriented LSR and RSR multilayers were subsequently equilibrated at various RH at 5°C over the 86–93% range for use in swelling experiments. Typically, a 5% change in RH, e.g., 88 vs. 93% RH, resulted in a 6–7% change in the multilayer periodicity of the various RSR and LSR multilayers. For the preparation of SR lipid multilayers, lipid was extracted from isolated SR vesicles with chloroform-methanol 2:1 (2) and dried under nitrogen. Medium I was added to the dried lipid

extract to yield a suspension (0.4 mg SR lipid/ml) that was sonicated in an ice bath and subsequently centrifuged and partially dehydrated at 93% RH, 5°C.

EQUIPMENT DESIGN All x-ray diffraction data were collected utilizing the equipment described (14). In these experiments, the guard-slit micrometers were set typically at 160–200 × 750 μm(width × height).

SPECIMEN GEOMETRY AND DATA DETECTION Alignment of the oriented RSR and LSR membrane multilayers with respect to the x-ray beam and diffraction data collection was similar to that used for highly purified SR (14). Determination of the water content of the membrane multilayers was the same as previously described (14).

DATA REDUCTION The lamellar diffraction on films was traced with a Joyce-Loebl microdensitometer using a fixed slit height of 0.5 mm, scanning through the center of each arc along the lamellar axis (Joyce-Loebl and Co., Ltd., Gateshead-on-Tyne, England). The relative height of the slit was small with respect to the degree of arcing (i.e., the mosaic spread) of the lamellar diffraction from RSR multilayers which was less than that of LSR multilayers. In the case of RSR multilayers, the background scattering was easily estimated from the scattering obtained from blank slides (19) and the non-Bragg lamellar scattering from highly ordered lecithin multilayers owing to the relatively low noise level of the low-angle lamellar diffraction data (see Fig. 2 for a typical microdensitometer tracing). The lamellar diffraction, corrected for background scattering (14), contained several zero-level minima.

The background-corrected lamellar diffraction data from all RSR and LSR multilayers investigated exhibited the effects of multilayer lattice disorder to varying degrees. For those multilayers with relatively greater lattice disorder, the various diffraction maxima all had widths (FWHM) greater than the camera linewidth and the data were digitized at intervals of $s = 5 \times 10^{-4}$ Å^{-1}, where $s = (2 \sin \theta)/\lambda$ is the reciprocal space coordinate. For those multilayers with lesser lattice disorder, their lower-angle lamellar diffraction consisted of several Bragg-like reflections, i.e., their widths were equal to the camera linewidth. In these cases, the integrated intensity values of these reflections at $s = h/D$, where h is the reflection order index and D is the multilayer periodicity, were also calculated from the similarly digitized data.

Neutron Diffraction Studies

PREPARATION OF HYDRATED ORIENTED MEMBRANE MULTILAYERS RSR samples (5–6 mg) were resuspended in medium I and oriented membrane multilayers were prepared as described above. These multilayers were equilibrated over the same relative humidity range used for the x-ray diffraction studies at 5°C. The saturated salt solutions were prepared at different D_2O/H_2O ratios, namely 100, 75, 25, and 0% D_2O allowing partial dehydration and H_2O-D_2O exchange of the samples to be carried out simultaneously.

After equilibration, the multilayers were quickly transferred to a temperature-regulated specimen chamber, which was pre-equilibrated and maintained throughout the neutron experiments at 7.5 ± 0.1°C. The entire specimen chamber was mounted on a goniometer on the ω-axis of the Brookhaven low-angle diffractometer (20).

EQUIPMENT DESIGN Lamellar neutron diffraction data were collected at the high flux beam reactor using the Brookhaven low-angle diffractometer operating at 2.36 Å (21). Incident beam dimensions were fixed at 1 × 3 mm (width × height) via adjustable slits on each end of a collimator (71.1 cm length), which permitted a full beam divergence of 0.161° to impinge on the multilayer. The monochromatic beam (graphite monochromator, $\Delta\lambda/\lambda = 0.04$) flux was $\sim 10^6$ cps/cm^2. The two-dimensional position-sensitive counter has a spatial resolution of 1.5 mm in the meridional (horizontal) direction and 3.0 mm in the equatorial (vertical) direction with a usable counting rate of 10^5 neutrons/s. A helium path was provided from the specimen to the surface of the position-sensitive counter.

SPECIMEN GEOMETRY AND DATA ACQUISITION The multilayers were aligned with respect to the neutron beam via ω-scans of the stronger lamellar reflections. Lamellar diffraction data (0.003 Å$^{-1} \leq s \leq 0.0250$ Å^{-1}) were collected at a specimen to detector distance of 220 cm via ω-scans ($-1° \leq \omega \leq 3°$; $\Delta\omega = 0.2°$); one complete ω-scan required on the order of 2 h. Several such ω-scans were taken over a period of 4–8 h.

DATA REDUCTION Lamellar diffraction data collected on the two-dimensional position-sensitive counter (22) was displayed as the number of counts vs. position in x (meridional) and y (equatorial) and showed the extent of the reflections for each ω-value. Appropriate summations provided the total integrated lamellar intensity function. The background scattering was estimated as described above for lamellar x-ray diffraction data and appropriately scaled to and subtracted from the total lamellar intensity function.

Electron microscopy studies

PREPARATION OF HYDRATED ORIENTED MEMBRANE MULTILAYERS Isolated LSR and RSR vesicle dispersions (~1 mg) were diluted in medium I and partially dehydrated membrane multilayers were prepared as described above. Following partial dehydration, a vial of 4% OsO_4 solution was placed in the sample container and *slow* fixation of these multilayers by osmium vapor proceeded for ~12 h. These samples were then counter-stained with 1% uranyl acetate, dehydrated, and embedded according to the usual procedures (13) with counterstaining and dehydration carried out simultaneously.

Alternatively, LSR dispersions (1 mg) were diluted in a final volume of 2.5 ml of medium I plus 100 mM sodium cacodylate (medium II). After slow partial dehydration, oriented multilayers were soaked in a fixing solution containing 1% tannic acid, 3.5% glutaraldehyde, 100 mM sodium cacodylate, pH 7.2 at 5°C for 1 h and washed three times in medium II (13, 23). Samples were then partially dehydrated for 12 h, after which time they were fixed by OsO_4 vapor, counter-stained, dehydrated and embedded in Spurr as described above.

Thin sections were cut approximately parallel to the sedimentation axis of the multilayer on an LKB Ultratome (LKB Instruments, Inc., Rockville, Md.) with diamond knives (E.I. DuPont de Nemours & Co., Wilmington, Del.), and subsequently examined in a Hitachi HU-11B electron microscope (Tokyo, Japan).

Materials

Glutaraldehyde (vacuum distilled and treated to remove traces of glutaric acid) was obtained from Polysciences, Inc. (Paul Valley Industrial Park, Warrington, Pa.). Spurr, Epon 812, and OsO_4 were purchased from Polysciences, Inc. Tannic acid and uranyl acetate were obtained from Mallinckrodt Inc. (St. Louis, Mo.).

RESULTS AND ANALYSIS

Physical Nature of RSR in the Dispersions Used for Preparing Oriented Multilayers

The dissociation of SR and reconstitution to form RSR has been shown to yield closed unilamellar membraneous vesicles, as viewed in the electron microscope using various fixation and staining techniques (13). Quasielastic light scattering measurements described in the previous paper (1) have shown that the average vesicle diameter is comparable to that observed in isolated LSR. These various RSR vesicle preparations with different L/P ratios are each homogeneous since they form a tight band on a continuous sucrose gradient. The statistical spread for a specified L/P molar ratio of RSR, as calculated from the width and density of this band, was found to be ±1%. The possibility that the reconstitution technique has led to the formation of either sheets or random sided vesicles may be excluded on the basis that RSR with L/P ratios comparable to that of LSR are capable of steady-state Ca^{2+} accumulations up to 90% that of LSR with 80% of the velocity and 70% of the efficiency of Ca^{2+} uptake for LSR (1). Thus, our hydrated oriented multilayers are prepared from closed, membraneous, unilamellar vesicles.

Nature of the Lamellar X-ray Diffraction from LSR and RSR Membrane Multilayers

Inspection of the lamellar x-ray diffraction from oriented RSR multilayers indicated that the 86–93% RH range and the 5–10°C temperature range was optimal. These RSR multilayers ($40 \leq L/P \leq 135$) contained typically 20–30% water by weight at 90% RH except for $L/P >$ 175 where the water content was 50–60%.

In Figs. 1 and 6, x-ray diffraction patterns characteristic of two different RSR multilayers and the SR lipid multilayer are shown at two different multilayer-to-film distances for the same relative humidity (93%). The mosaic spread of these multilayers, as estimated from the degree of arcing of the lamellar diffraction maxima, ranged typically from ±10° to ±15° at 93% RH. A microdensitometer tracing of a typical diffraction pattern is shown in Fig. 2 and corresponds to the data set used as an example in the analysis section below. The low and high angle lamellar diffraction data from this RSR multilayer is seen to lie on a low background scattering (dotted line) which was estimated as described above. It is evident from the low-angle ($s \leq 0.0500$ Å^{-1}) lamellar diffraction data that the low background scattering from RSR multilayers mainly arises from camera background scattering, since it rapidly decays, being almost nonexistent at $s > 0.0200$ Å^{-1}. In contrast, for isolated LSR (14), the multilayer specimen itself contributes to the lamellar incoherent scattering (diffuse lamellar scattering), thus adding to the camera background scattering and yielding a much greater total apparent background scattering. This is probably a result of the greater homogeneity of the RSR preparations over that of isolated LSR.

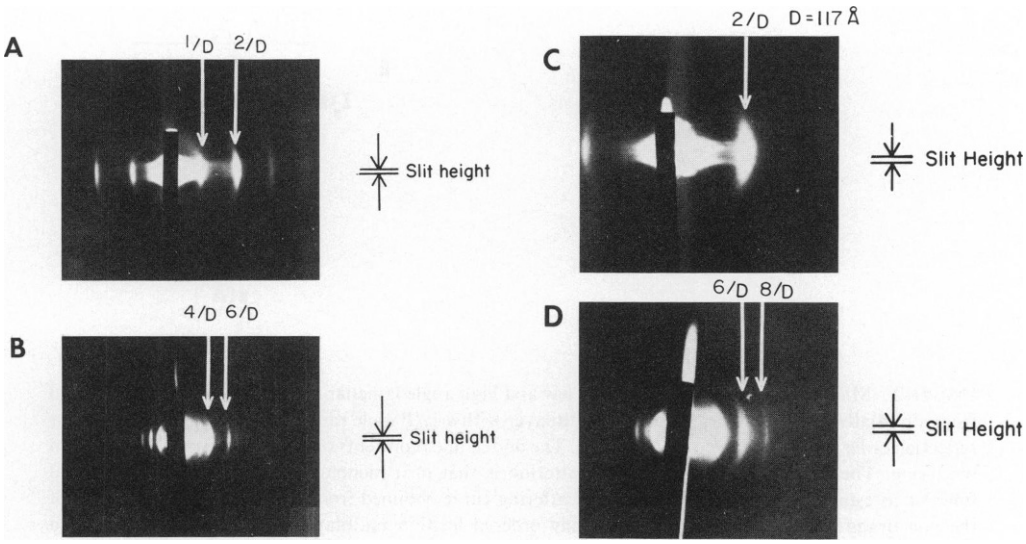

FIGURE 1 (*A*) A lower angle x-ray diffraction pattern of a partially dehydrated oriented multilayer of RSR membranes (L/P mole ratio = 104.9) taken at 93% RH and 5°C. (*B*) A higher angle diffraction pattern from the same specimen as in (*A*). The "equatorial" diffraction maximum at $x \simeq 1/10$ Å, which extends to the lamellar axis, can be seen on the original film. (*C*) and (*D*) Corresponding x-ray diffraction patterns for RSR with an L/P mole ratio equal to 129.2. The actual slit height (0.5 mm) set on the microdensitometer at the position of the film and used to scan the lamellar axis is shown relative to the lamellar diffraction in *A–D*.

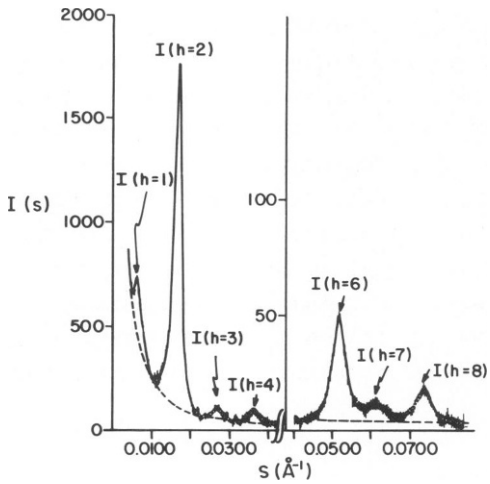

FIGURE 2

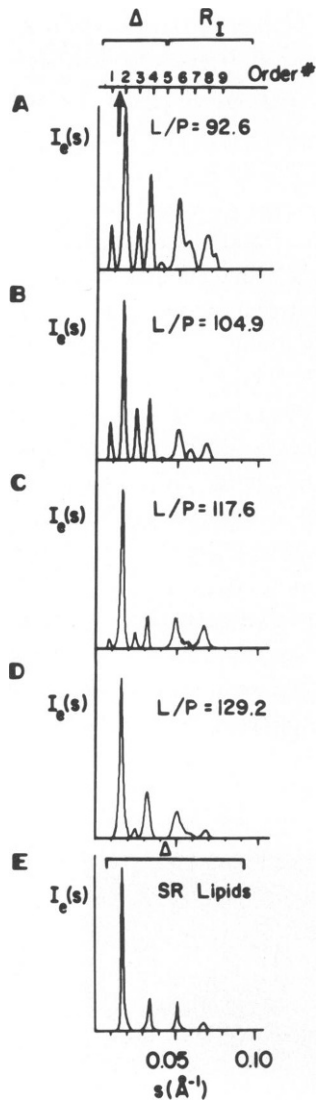

FIGURE 3

FIGURE 2 Microdensitometer tracing of the low and high angle lamellar x-ray diffraction data obtained from a partially dehydrated oriented RSR multilayer with a L/P mole ratio equal to 117.6. The lamellar reflection order number is labeled in each case. The dotted line represents the scaled estimated background scattering. The *shape* of the background scattering is that of a monotonically decreasing exponential function as estimated from the shape of the scattering curve obtained from blank slides and the shape of the non-Bragg lamellar scattering from highly ordered lecithin multilayer specimens. This estimated background scattering curve was scaled to the total lamellar diffraction so as to produce the maximum number of zero-level minima in the background corrected lamellar diffraction. These zero-level minima are expected, since electron microscope images revealed that the unit cell profile of the RSR multilayer contains two apposed membrane profiles of the flattened RSR vesicle producing a center of symmetry in the unit cell profile which requires the background-corrected lamellar diffraction to contain zero-level minima; the maximization of the number of such minima is essential in order to ensure that the maximum number of possible phase combinations will be explored by the phasing procedure utilized. The open circles through the diffraction maxima represent a simple smoothing of the local noise.

FIGURE 3 Corrected experimental lamellar intensity functions from RSR multilayers with L/P > 88 (*A–D*). In (*E*), the lamellar intensity function for purified SR lipids is shown for comparison. The least-squares fit parameters, Δ and R_I, are indicated over those regions of reciprocal space for which they were calculated.

Before analysis, the lamellar x-ray diffraction from the various RSR multilayers was corrected for background scattering and subsequently corrected by a factor of s^2, where $s = (2 \sin \theta)/\lambda$ is the reciprocal space coordinate. One factor of s is a correction for the intersection of the reciprocal lattice for the multilayer with the Ewald sphere arising from the cylindrical curvature of the multilayers and the other factor of s is an approximate microdensitometry correction arising from scanning the lamellar x-ray diffraction patterns along the lamellar axis with a slit height which was small compared to the degree of arcing of the lamellar diffraction maxima. This latter correction has been experimentally shown to be a reasonably good approximation (14).

These corrections provided the corrected experimental lamellar intensity function, $I_e(s)$, which is shown for various RSR multilayers investigated as a function of L/P ratio in Fig. 3. Inspection of these $I_e(s)$ intensity functions shown in Fig. 3 indicated that all of the various RSR multilayers possess lattice disorder since the widths of the various maxima in $I_e(s)$ increase monotonically with increasing reciprocal space coordinate s (24). The apparent degree of lattice disorder in these RSR multilayers is less than found for LSR (14) since the lower angle maxima have widths nearly equal to the camera linewidth. Furthermore, the RSR multilayer periodicity, D, determined from the reciprocal space coordinates of the lower-angle lamellar diffraction maxima that could be indexed on a one-dimensional reciprocal lattice for all L/P ratios investigated, was similar for all preparations with L/P > 88 as is readily apparent in Fig. 4, where D is plotted versus L/P ratio. (Results obtained for RSR preparations with L/P < 88 may be found in Appendix A.)

Physical Nature of LSR and RSR Membrane Multilayers

1. ISOLATED LSR *a) Electron microscopy of LSR multilayers* Examination of appropriate thin sections (using either fixation procedure) (13, 25, 26) of the LSR multilayer reveals the profiles of stacks of flattened vesicles within the multilayer as indicated primarily

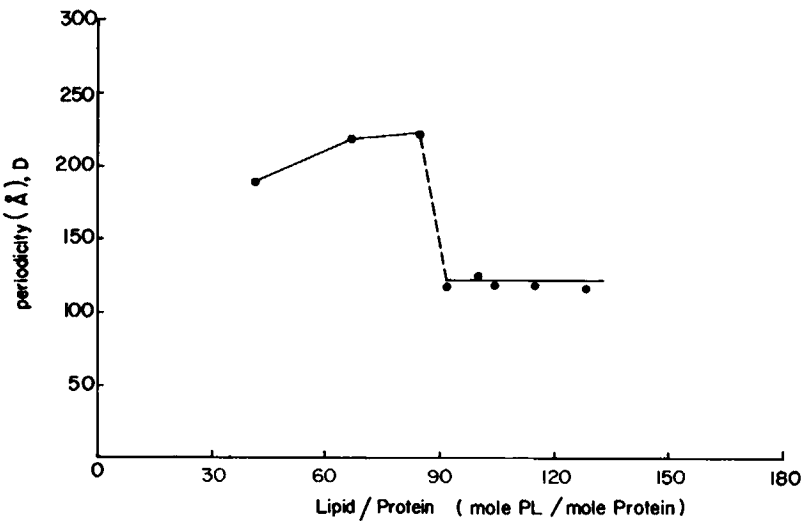

FIGURE 4 The multilayer periodicity, D, vs. L/P mole ratio. The unit cell profile (see Fig. 9) of the multilayer contains the membrane pair of the flattened RSR vesicle.

by the repeating pattern of alternate thick and thin electron opaque bands in Fig. 5*A1*. The periodicity of the multilayer banding pattern is 170–180 Å and one unit cell[2] is indeed seen to contain the profile of one flattened vesicle when one follows the image of the fixed membrane profile around the edge of the flattened vesicle. Hence, the unit cell profile for LSR oriented multilayers should be centrosymmetric.

The separation of the centers of the membrane profiles (seen as the electron translucent bands in the micrograph) within one vesicle is $\sim D/4 - D/3$. These results are in good qualitative agreement with those of x-ray and neutron diffraction studies by Herbette et al. (14, 27).

b) Lamellar x-ray intensity function of LSR multilayers The lamellar diffraction data from hydrated oriented multilayers of LSR vesicles showed monotonically increasing widths for higher order lamellar reflections, indicative of simple lattice disorder within the multilayer (14, 24). The lamellar intensity function at higher-angle contained no lattice interference effects, therefore varying as the square of the unit cell structure factor modulus $|F_{uc}(s)|^2$ for $s > 8/D$, and contained several zero-level minima. The wavelength of the fluctuations in $|F_{uc}(s > 8/D)|^2$ was substantially greater than that of the square of the single membrane structure factor modulus $|F_{sm}(s)|^2$, of $\sim 1/40$ Å for LSR, which may be obtained from the scattering from unilamellar vesicular dispersions (28). Hence, the nature of this higher angle lamellar diffraction data indicates that the multilayer unit cell profile cannot contain only a single membrane profile (as would be the case for stacks of membrane sheets and flattened "vesicles within vesicles"). Consideration of multilayer water content and periodicity would indicate that the unit cell profile contains the two apposed membrane profiles of a flattened unilamellar vesicle.

Hence, both the nature of the lamellar x-ray diffraction at higher angles and the electron microscopy indicate the predominance of stacks of flattened vesicles within LSR oriented multilayers justifying the adoption of centrosymmetric phases for the lamellar diffraction.

2. RSR FOR L/P > 88 *a) Electron microscopy of RSR multilayers* Examination of appropriate thin sections of RSR multilayers for L/P ratios >88 (e.g., L/P = 122.7, as shown in Fig. 5*B1*), reveals the profiles of stacks of flattened vesicles within the multilayer, as indicated by the repeating pattern of alternate thick and thin electron opague bands. The unit cell profile of this multilayer again contains the two membrane profiles of the flattened vesicle and a resulting center of symmetry; the multilayer periodicity in this typical case is ~102 Å, and the separation of the centers of the membrane profiles within the vesicle is $\sim 0.4D$.

b) Lamellar intensity functions of RSR Lamellar diffraction from RSR reveals that systematic changes occur in the various $I_e(s)$ functions vs. L/P molar ratio, as can be readily observed in Fig. 3 *A–D*. The appearance and subsequent systematic increase in the relative intensities of the odd order maxima at lower angle upon decreasing the L/P ratio from that of

[2]Owing to the nature of the corrected lamellar intensity data, the calculated and experimental truncated unit cell electron density profiles i.e., $\rho_e(x)$ and $\rho_e(x)$, produced by the GFSDM, appear virtually superimposable in Figs. 9 and 11 and almost superimposable in Fig. A2(*B*), over this range: $-D/2 \leq x \leq D/2$. Therefore, no attempt was made to separate these calculated functions so that any small deviations would be more easily recognized in the analysis of the data. The crystallographic unit cell for all RSR and SR multilayers was found to contain two asymmetric membranes corresponding to the two apposed membranes of the flattened vesicle. For purified SR lipids, only, the unit cell contained one symmetric membrane.

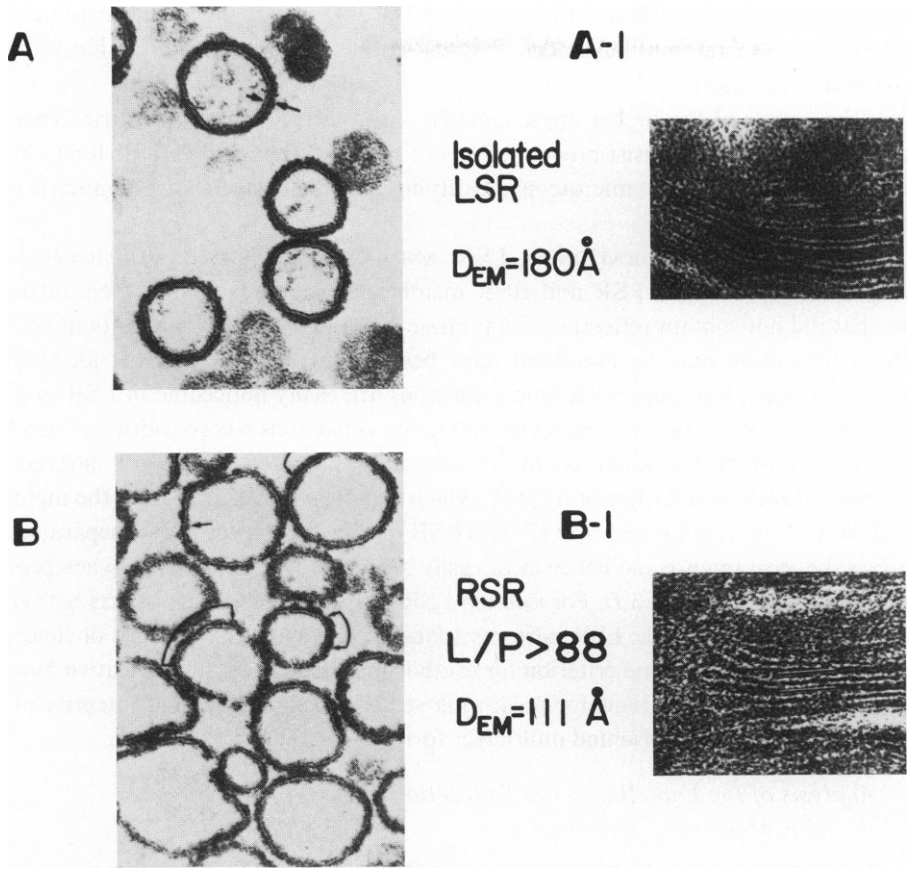

FIGURE 5 (*A*) Electron micrograph of membraneous vesicles of isolated LSR fixed via the tannic acid-osmium method. The arrows indicate the localization of heavy staining exclusively in the extravesicular half of the LSR membrane for those regions of the membrane profiles in the plane of thin sectioning. In *A-1*, an electron micrograph of a hydrated oriented membrane multilayer of the same preparation fixed via the osmium vapor method is shown. The unit cells containing the two apposed membranes of the flattened vesicle have a profile dimension of ~180 Å. Similar experiments were carried out with RSR (*B*, *B-1*). In *B* the bracketed arrows indicate the predominant localization of heavy staining in the extravesicular half of the RSR membrane as observed in LSR with the occasional appearance of heavy staining in the intravesicular half of the membrane for those regions of the membrane profiles in the plane of thin sectioning.

a pure SR lipid bilayer accompanied by smaller changes in the relative intensities of the even-order maxima using either x-rays or neutrons strongly indicates that the multilayer unit cell profile contains the two apposed membrane profiles of one flattened RSR vesicle with a resulting center of symmetry; multilayers composed of vesicles within vesicles or membrane sheets diffract as if there were essentially only one membrane in the multilayer unit cell (10), which, for these RSR multilayers, is inconsistent with their larger periodicities and lower water contents, as compared with the pure SR lipid multilayer. In addition, the higher angle lamellar diffraction, where lattice interference effects are virtually absent because of the degree of multilayer lattice disorder (e.g., $s > 0.04$ Å^{-1} in Fig. 3 *A*, *B* and *D*) contains several

zero-level minima and fluctuates with a wavelength $\leq 2/D$, which is also inconsistent with a substantial portion of the multilayer being composed of flattened vesicles within vesicles or stacks of membrane sheets.

Hence, the nature of the higher angle lamellar x-ray diffraction also confirms that these RSR oriented multilayers consist predominantly of stacks of flattened vesicles for $L/P > 88$, in agreement with the electron microscopy, justifying the adoption of centrosymmetric phases for the lamellar diffraction.

3. LIPID PHASE SEPARATION IN LSR AND RSR MEMBRANE MULTILAYERS All scattering density profiles of LSR and RSR membranes were determined from diffraction patterns that did not contain reflections from phase-separated lipid. The conditions by which lipid phase separation may be prevented have been outlined in Herbette et al. (14). The appearance of these phase separated lipid reflections are easily noticeable in LSR and RSR diffraction patterns since they appear as sharp intense reflections whose width and height are comparable to that of the x-ray beam. In addition, these reflections are indexed on a one-dimensional reciprocal lattice of $h/55$ Å, which is quite well resolved from the membrane lattice of $h/157$ Å (LSR) and $h/117$ Å (RSR). The first-order phase-separated lipid reflection is the most intense and hence most easily recognized and its position when present is indicated by the arrow in Fig. 3 *D*. For isolated LSR this same reflection appears between the second and third orders of the LSR patterns (data not shown). The absence of lipid phase separation has been used as one criterion for establishing the temperature, relative humidity, ionic strength, pH, etc. conditions for preserving structural and functional integrity of LSR and RSR membranes in the oriented multilayer form.

Analysis of the Lamellar X-ray Diffraction from the RSR Membrane Multilayers

1. ELECTRON DENSITY PROFILE OF THE SR LIPID BILAYER Lamellar x-ray diffraction from purified SR lipid multilayers was obtained at three relative humidities (81, 88, and 93%); the diffraction pattern at 93%, RH is shown in Fig. 6. The corrected lamellar intensity functions for the three sets of lamellar diffraction data contained only Bragg-like reflections which could be indexed on a one-dimensional reciprocal lattice, thereby providing the three multilayer periodicities. Applying the so-called swelling method (29) using the algorithm of Stamatoff and Krimm (30), the lamellar reflections shown in Fig. 6 *A* and *B* were phased by utilizing, for example, the 81 and 93% RH data, which yielded the most probable unit cell electron density profile for the SR lipid multilayer shown in Fig. 6 *C*. This algorithm provides a hierarchy of more probable unit cell profiles, the most probable profile possessing the least deviation with variations in multilayer periodicity. Stamatoff and Krimm (30) showed that the ordering within such hierarchies was unaffected by the introduction of 10% random errors in the lamellar intensity data. Since the experimental errors in the lamellar intensity functions for the SR lipid multilayers are estimated to be significantly $<10\%$, the most probable profile calculated using this algorithm should be the correct profile.

2. ELECTRON DENSITY PROFILES OF RSR MEMBRANES, $L/P > 88$ Inspection of Fig. 3 *A–D* clearly indicates that the lower angle lamellar diffraction maxima ($s \leq 0.04$ Å^{-1}) are generally only slightly greater than the diffraction camera linewidth for these RSR multilayers (the widths of the first three diffraction orders obtained from SR lipid multilayers, i.e., $h = 1$–3, in Fig. 3 *E* are the camera linewidth). This fact, together with the

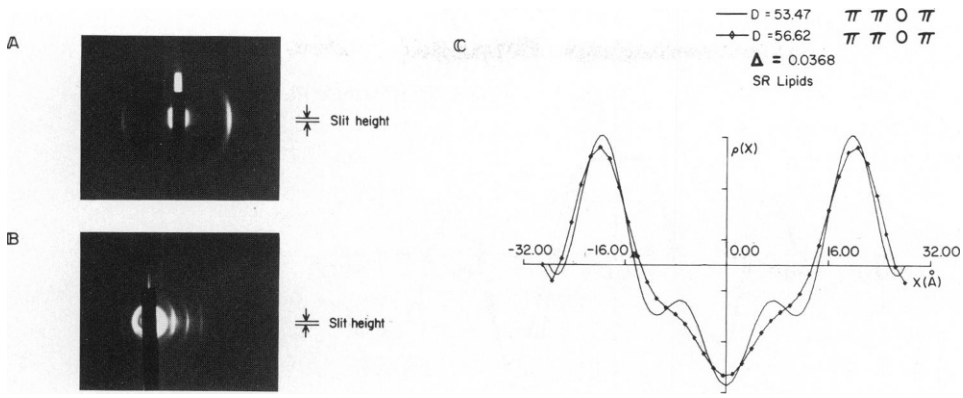

FIGURE 6 (*A*) and (*B*) An x-ray diffraction pattern of a partially dehydrated oriented multilayer of purified SR lipids at 93% RH and 5°C, showing the low- and high-angle lamellar reflections, respectively. (*C*) Superposition of electron density profiles of SR lipids at two different RH (81 and 93%) phased by the swelling method. Swelling is seen to occur predominantly at the edges ($\pm D/2$) of the unit cell which contains one symmetric membrane.

relatively small degree of lattice disorder determined for these multilayers ($\gamma/D < 0.05$, [24]), would suggest utilizing the swelling method to derive the most probable low-resolution unit cell electron density profile. In Table I, the hierarchy of the first three more probable phase combinations (along with their corresponding Δ values [the measure of the deviation of the correspondingly phased profile with the variation in multilayer water content]) are given for the lower angle lamellar reflections, $I_e(h = 1\text{–}4)$ for L/P = 117.6. These differences in Δ values are significant, since the experimental errors for the lower angle lamellar reflections are estimated to be considerably <10% (see section 1 above). With the phases of the lower angle maxima assigned (000π), (the corresponding low-resolution unit cell electron density profile is shown in Fig. 7), the phasing procedure was extended to higher angle. Examination of the corresponding higher angle lamellar diffraction data shown in Fig. 3 *A–D* from these RSR multilayers reveals the presence of a certain amount of lattice disorder in these multilayers, which was sufficient to cause not only broadening of these lamellar diffraction

TABLE I
LOW RESOLUTION Δ-VALUES

	Phase assignments (h)				Δ
	1	2	3	4	
$\Phi_1(h)$	0	0	0	π	0.0771
$\Phi_2(h)$	0	0	0	π	
$\Phi_1(h)$	π	0	0	π	0.0782
$\Phi_2(h)$	π	0	0	π	
$\Phi_1(h)$	π	0	0	0	0.0969
$\Phi_2(h)$	π	0	0	0	

$\Phi_1(h)$ and $\Phi_2(h)$ are the phase assignments of the lamellar reflections corresponding to each of the multilayer unit cell repeat distances upon swelling of the multilayer.

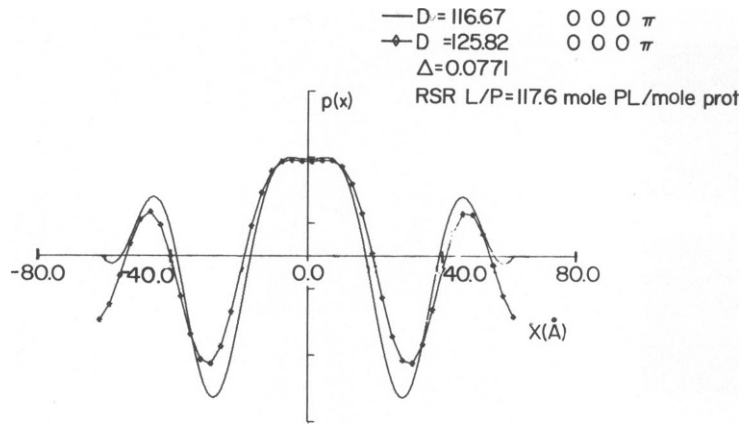

FIGURE 7 Superposition of the low resolution (30 Å) electron density profiles of RSR with a L/P ratio = 117.6 at two different relative humidities (88 and 93%) phased by the swelling method. Swelling is seen to occur predominantly at the edges ($\pm D/2$) of the unit cell which contains the two apposed asymmetric membranes of the flattened RSR vesicle. The hydrocarbon core of each bilayer located about $x = \pm 29$ Å is clearly revealed in these low resolution profiles with the inner phospholipid headgroups barely resolved and centered about $x = 0$.

maxima, but also shifting of some of the maxima from their ideal reciprocal lattice positions at $s = h/D$ and the presence of nonzero minima in the lamellar intensity function. Consideration of the generalized Fourier series deconvolution method (GFSDM) phasing procedure (24) indicates that this method may be used in reciprocal space to phase these less intense, higher angle lamellar diffraction maxima because the variation of the phases of the higher angle maxima would conversely be delocalized over the calculated Q-function $Q_c(x)$ in real space, and therefore a real-space GFSDM analysis might be less suitable for distinguishing the most probable profile. However, the higher angle data were phased by considerations of both the least-squares fit of the various $I_c(s)$ and $Q_c(x)$ functions, corresponding to the various possible phase combinations for the higher angle diffraction maxima, to the experimental $I_e(s)$ and $Q_e(x)$ functions (so-called R_I and R_Q fits respectively) obtained by the GFSDM analysis. In Table II, the hierarchies of the R_Q and R_I fits are given for the various possible phase combinations listed and both indicate that the phase combination no. 29 ($000\pi\pi\pi$) is the most probable for L/P = 117.6. In addition, we allowed the phase of $I_e(h = 1)$ to vary since the results of the swelling method in Table I indicated that the second smallest Δ value was obtained when this phase was π, due to the relative low intensity of this reflection with respect to the other lower-angle reflections; also the phase of the last reflection in the lower-angle data [in this case $I_e(h = 4)$] was varied because of a possible effect of the phases of the higher lamellar data on the phase of the neighboring $I_e(h = 4)$ reflection based on considerations of the Fourier sampling theorem. However, both the R_Q and R_I fits for all of the resulting possible phase combinations obtained via the GFSDM analysis were substantially greater than those shown in Table II, in which the phases of the first four reflections were the most probable as determined by the swelling method.

We note that the R_I value for the most probable phase combination no. 29 for L/P = 117.6 ($000\pi\pi\pi$) is significantly different statistically from the first three more probable phase combinations in Table II (and therefore all others) as demonstrated in detail in Fig. 8.

TABLE II
HIGH RESOLUTION R_Q AND R_I-VALUES* CALCULATED BY THE GFSDM

Phase combination	$R_Q(0 \rightarrow 117$ Å)	$R_I(0 < s < 0.075$ Å$^{-1})$
29 ($000\pi\pi\pi$)	0.0150	0.0470
5 ($000\pi00$)	0.0160	0.0540
21 ($000\pi0\pi$)	0.0190	0.0560
13 ($000\pi\pi0$)	0.0200	0.0530

*Beamwidth was convoluted into the interference function before analysis.

Therefore, the corresponding most probable unit cell electron density profile so derived and shown in Fig. 9 *c* for L/P = 117.6 is the correct profile. The lamellar diffraction data from other RSR multilayers for L/P > 88 were analyzed independently according to this procedure and have provided the other most probable unit cell electron density profiles given in Fig. 9.

A summary of the most probable phase assignments for the various RSR multilayers in the L/P regime considered here are given in Table III, along with that of the SR lipid multilayer (the phases for the SR lipid multilayer have been adjusted to correspond to the situation of two lipid bilayers in a unit cell profile of dimension $2D$ in order to allow a direct comparison with the phases of the RSR multilayers in this L/P regime, i.e., $[\pi\pi0\pi]$ for orders h = 1–4 become $[0\pi\pi\pi]$ for orders h = 2, 4, 6, 8). The absence of an assignment indicates that the corresponding diffraction maximum was not experimentally observed. It is immediately evident that the above procedure applied independently to the lamellar diffraction data from these various RSR multilayers has led to the same phasing of the lamellar diffraction maxima observed, i.e., the phase assignments for the various regions of reciprocal space are identical for the various RSR multilayers. Inspection of the lamellar intensity functions in Fig. 3 *A–D* for these four RSR preparations indicate that the continual increase in incorporation of the Ca^{2+} pump protein into the SR lipid bilayer results in a progressive increase in the amplitude of the odd order lamellar diffraction maxima consistent with an increase in the degree of asymmetry observed in the profiles for $0 \leq |x| \leq D/2$, shown in Fig. 9.

3. DETERMINATION OF RSR MEMBRANE ELECTRON DENSITY PROFILE WITH RESPECT TO OVERALL SIGN In the case of RSR multilayers with L/P > 88, comparison of the unit cell electron density profiles shown in Fig. 9 *A–D* with that of the SR lipid profile would indicate that the overall sign of these RSR membrane profiles is correct, as shown in Fig. 9. The correct overall sign of the typical lipid bilayer electron density profile (31) as shown in Fig. 9 for the SR lipids is well established from simple considerations of the nature of lipid bilayer structures. The similarity of the RSR multilayer unit cell profile within $0 \leq |x| \leq D/2$ for the larger L/P ~128 with the SR lipid profile, establishes its overall sign. Since the increasing incorporation of protein into the SR lipid bilayer for RSR membranes produces only systematic changes in the lamellar x-ray diffraction from the multilayers, we would expect only systematic changes in the derived RSR multilayer unit cell profiles, as shown in Fig. 9 *D* → *A*, their overall sign thereby being correct, as shown in Fig. 9.

Lamellar Neutron Diffraction from RSR Membrane Multilayers

Typical examples of the lower angle lamellar neutron diffraction from these RSR multilayers may be found in Fig. 10 *A*; the multilayer periodicities were determined from the positions of

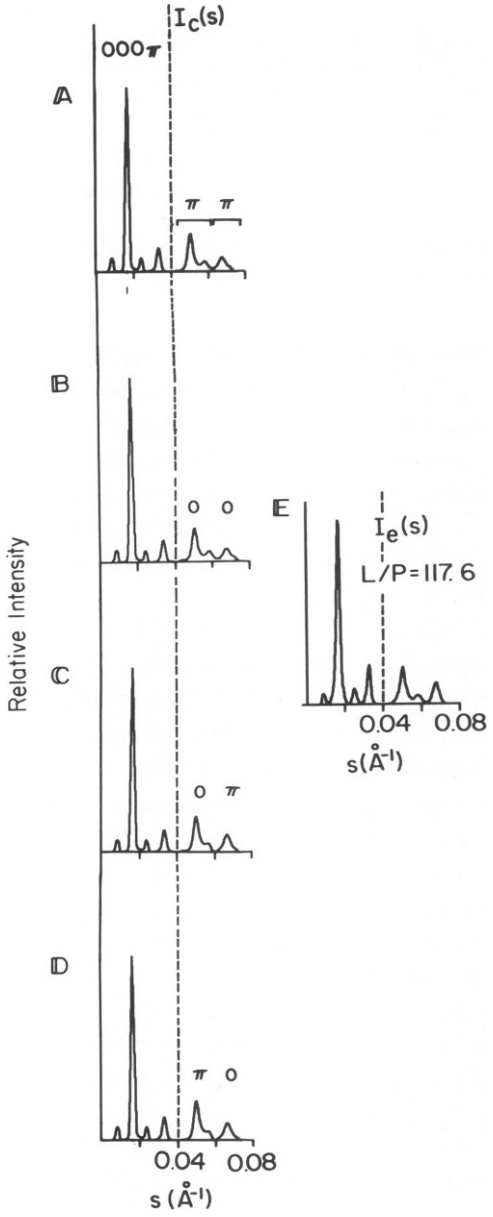

FIGURE 8

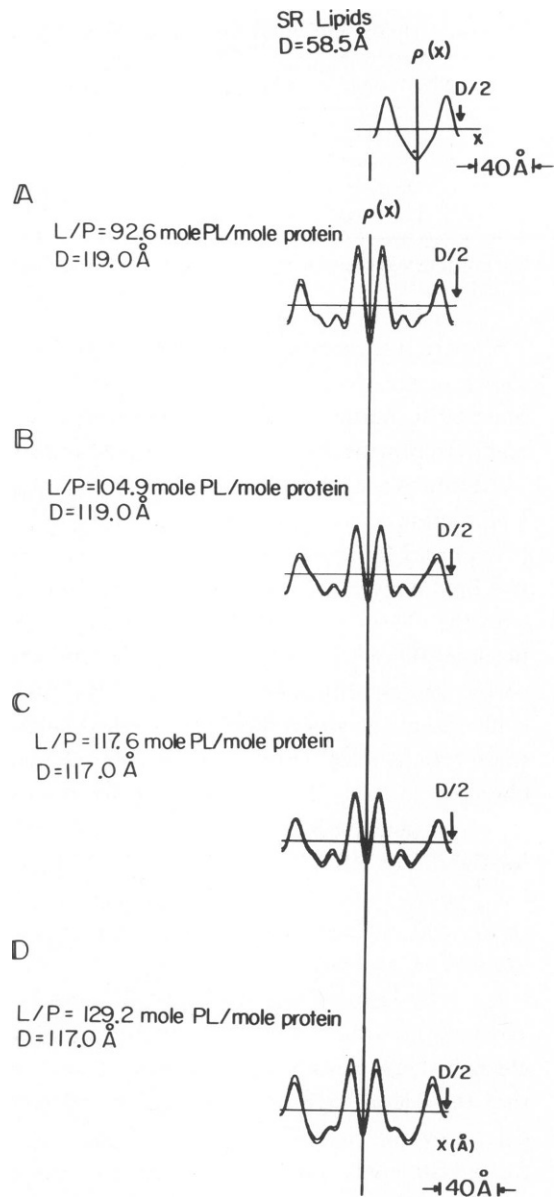

FIGURE 9

FIGURE 8 Calculated lamellar intensity functions $I_c(s)$ corresponding to the first four more probable phase combinations generated by the GFSDM analysis. The experimental intensity function $I_e(s)$ for RSR and L/P = 117.6 is shown in *E* for comparison. Comparison of these four calculated intensity functions with the experimental intensity function via simple inspection reveals that when the last two maxima [$0.04 \leq s(\text{Å}^{-1}) \leq 0.07$] have different phases (*C*, *D*), the form of the calculated intensity functions differs substantially from that of the experimental intensity function in the vicinity of $I(h = 7)$. Specifically, the position of the $I(h = 7)$ maximum, accurately determined from Fig. 2, is clearly predicted incorrectly when the last two maxima have different phases. These differences are greater than the experimental

TABLE III
PHASE ASSIGNMENTS FOR SR LIPIDS AND RSR L/P > 88

	Phase assignments (h)							
	1	2	3	4	5	6	7	8
SR Lipids		0		π		π		π
RSR (L/P)								
129.2		0	0	π		π		π
117.6	0	0	0	π		π	π	π
104.9	0	0	0	π	π	π	π	π
92.6	0	0	0	π	π	π	π	π

the lamellar reflections in reciprocal space. In this figure, the dotted line represents the background scattering. The lower angle lamellar neutron diffraction from these RSR multilayers was necessarily found to consist of Bragg-like reflections due to the larger camera linewidth of the low-angle diffractometer.

Analysis of the Lamellar Neutron Diffraction from RSR Membrane Multilayers

The total lamellar intensity functions were corrected for background scattering and subsequently by only one factor of s (Lorentz correction for ω-scans). Further corrections to the integrated lamellar reflections for absorption and (primary) extinction in the multilayer samples were found to be negligible. Calculation of the total attenuation coefficient for the RSR multilayer samples based on their compositions, according to Schoenborn and Nunes

errors [note the signal-to-noise levels and the positions of these high-angle maxima indicated in Fig. 2 for the $I_e(s)$ function]. The remaining two calculated intensity functions A and B, which have the same phases for these last two maxima, have nearly equivalent forms for the region $0.04 \leq s(\text{Å}^{-1}) \leq 0.07$, more similar to that of the experimental intensity function. However, the experimental ratio of the most significant low-angle reflection to the most significant higher angle maximum within $0.04 < s(\text{Å}^{-1}) < 0.07$, namely, $I(h = 2)/I(h = 6)$ of 4.9 ± 0.2, is best reproduced in the calculated intensity function for phase combination A (i.e., 4.9), as compared with phase combination B (i.e., 5.5). We note that the amplitude of the maximum $I(h = 8)$ has not been correctly predicted for any of these phase combinations A–D. The precise amplitude of the $I(h = 8)$ maximum in these calculated functions would necessarily be in greatest error due to the artificial truncation of the experimental lamellar diffraction in this region of reciprocal space. Owing to the intensity of the diffuse diffraction at $s \simeq 1/10$ Å, relative to lamellar reflections for $h > 8$, a considerable amount of uncertainty is introduced into the determination of the amplitude of the $I(h > 8)$ maxima, so that the lamellar intensity function was necessarily truncated beyond $I(h = 8)$ in this analysis. Therefore, the R_I value shown in Table III for phase combination A is significantly different *statistically* from those for phase combinations B, C, and D, since phase combination A can predict the experimental intensity function to within the experimental errors over a substantially greater range of reciprocal space, i.e., for $I_e(h = 1 \rightarrow 7)$. As a result of the above considerations, the most probable phase combination A provided by the GFSDM analysis is the correct solution for the experimental intensity function (Figs. 8 E and 2).

FIGURE 9 Electron density profiles of RSR membrane multilayers with L/P > 88 truncated at D/2 at 13 Å resolution. The L/P mole ratio, along with D, is indicated for each profile. The unit cell profile of the multilayer contains the membrane pair of the flattened RSR vesicle. Note the insert at the top right, showing the bilayer profile of purified SR lipids positioned over one asymmetric membrane profile of the RSR unit cell.

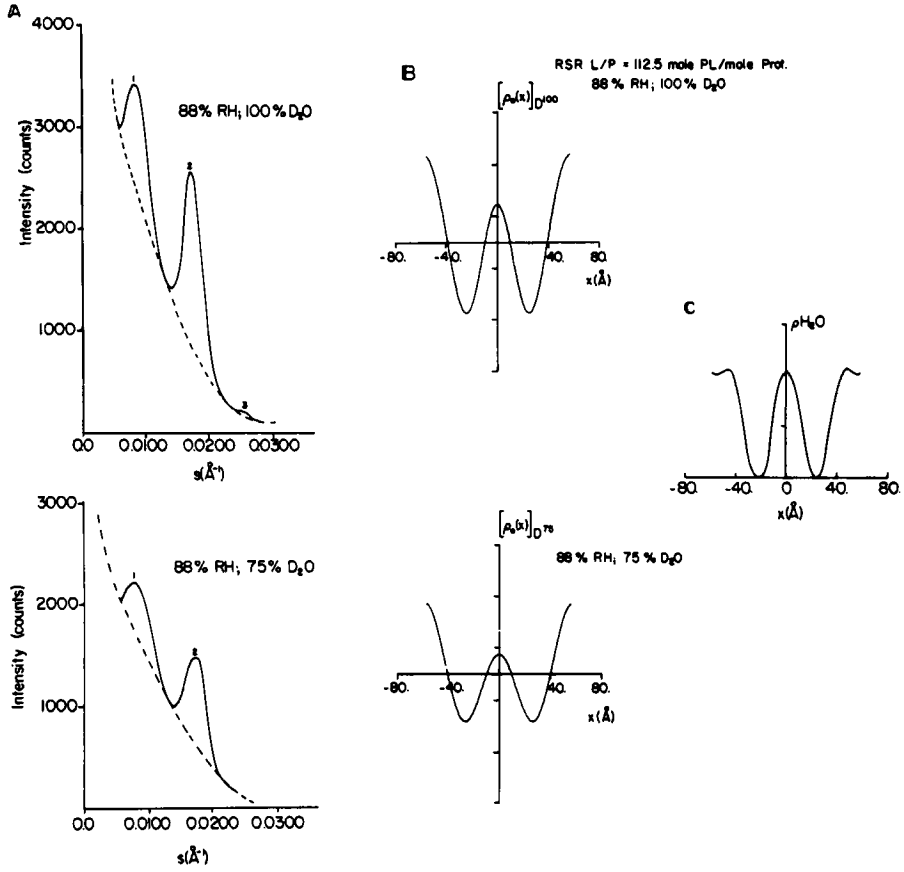

FIGURE 10 (*A*) Lamellar neutron diffraction patterns at two H_2O/D_2O ratios from an RSR membrane multilayer with L/P equal to 112.5. The dotted line represents the estimated background scattering curve. (*B*) Unit cell neutron scattering profiles calculated from the corresponding corrected lamellar intensities shown in (*A*). (*C*) The water profile of the RSR multilayer unit cell. The absence of water around $|x| = 0.2\ D$ reflects the location of the lipid hydrocarbon core of each RSR membrane in the unit cell which may be compared with the electron density profiles shown in Fig. 9.

(21), gave a typical value[3] of ~3.8 cm^{-1}. However, owing to the small differences in path length in the multilayers for the various lamellar reflections observed ($s < 0.025$ $Å^{-1}$) due to the relatively thick multilayer specimens, beam attentuation phenomena in these multilayers may be neglected. In addition the presence of primary extinction effects would cause the structure factor moduli obtained from the strongest (low-angle) reflections to have a nonlinear dependence on the amount of D_2O present in the multilayers in D_2O/H_2O exchange

[3]The value of μ given in the text was calculated for an RSR multilayer with L/P > 88 (e.g., L/P = 100 mol PL/mol prot) hydrated at 100% D_2O based on an average water content of 25% for this multilayer. For this same RSR multilayer hydrated at 75% D_2O, μ is 4.1; i.e., μ differs by <10% of the value at 100% D_2O. The value of μ for an RSR multilayer with L/P < 88 (e.g., L/P = 50 mol PL/mol prot) is 10% lower than its value for RSR with L/P < 88 at the same H_2O/D_2O ratio.

experiments (32). The observed linearity of the structure factor moduli vs. RSR multilayer D_2O content suggests that such extinction effects are not significant.

DETERMINATION OF THE UNIT CELL WATER PROFILE FOR RSR MEMBRANES (L/P > 88) The lower angle lamellar reflections obtained from RSR multilayers with a L/P ratio of 112.5 at 88 and 92% RH in 100% D_2O, viz., I (h = 1–3), were phased by the swelling method (29). The resulting phase assignment was (π00) for h = 1–3. With the H_2O/D_2O exchange of these multilayers to successively lower D_2O contents at 88% RH, it was determined that the phases of the lamellar reflections I (h = 1–3) did not change when the D_2O content was reduced to 75%. The total lamellar intensity functions and the corresponding unit cell neutron scattering profiles for this RSR multilayer of L/P = 112.5 in 100% D_2O and 75% D_2O, as derived from the phased lamellar reflections, are shown in Fig. 10 *A*, *B;* the derived profiles were computed using the standard Fourier series representation for the multilayer unit cell scattering profile and scaled to one another (8). The difference between these two scaled unit cell neutron scattering profiles is just the unit cell water profile for this RSR multilayer, as shown by Zaccai et al. (8). This derived unit cell water profile, ρ_{H_2O}, is also shown in Fig. 10*C*.

DISCUSSION

Profile Structure of the RSR Membranes

The general similarity of the unit cell electron density profile within $0 \leq |x| \leq D/2$ for RSR multilayers with L/P > 88 i.e., L/P = 128, with the SR lipid bilayer profile clearly indicates the presence of two asymmetric apposed membranes within the RSR multilayer unit cell profile. This membrane pair profile corresponds to that of the flattened RSR membrane vesicle, as evident from the electron microscopy studies of these multilayers. There are two major relatively electron-dense maxima in the single membrane profile. They are contained within $0 \leq |x| \leq D/2$ and are presumably associated with the phospholipid polar headgroups of the SR lipid bilayer within this RSR membrane profile. Their separation is around 40 Å, identical to that observed in the purified SR lipid profile. The region of relatively low electron density, centered about $|x| \simeq 0.23\ D$ and extending from $0.12\ D \leq |x| \leq 0.35\ D$, would then presumably contain the phospholipid hydrocarbon chains. These conclusions are in excellent agreement with the low-resolution unit cell water profile which indicates that water is excluded from the region about $|x| \sim 0.2\ D$ (~25 Å), the approximate center of the lipid hydrocarbon core of this RSR membrane profile. In addition, the same density of water is seen to be located in water layers about $x \simeq 0$ and $|x| \sim D/2$ in this profile, i.e., in the intravesicular and extravesicular spaces, respectively. The latter are identified as the water space about which lattice swelling and lattice disorder occurs. The extent of the extravesicular water space in the unit cell profile is seen to be somewhat greater than that of the intravesicular water space, in agreement with the unit cell electron density profiles.

The electron-dense maximum corresponding to the phospholipid headgroups at the extravesicular surface of this RSR membrane (nearest $|x| = D/2$) is seen to be slightly broadened and reduced in amplitude when compared with the maximum that corresponds to the phospholipid headgroups at the intravesicular surface (nearest $x = 0$); the width of the latter maximum is comparable to that for the polar headgroups in the purified SR lipid profile.

Furthermore, the lipid hydrocarbon core of this RSR membrane located throughout 0.12 $D \leq |x| \leq 0.35\ D$ is seen to be asymmetric, unlike that of the purified SR lipid profile, due primarily to an increase in electron density occurring in the extravesicular half of the hydrocarbon core of this RSR membrane. Further increases in the protein content of these RSR membranes (i.e., L/P decreasing from 129.2 to 92.6) resulted in a continual systematic increase in the electron density of the lipid hydrocarbon core of the RSR membranes. This was especially true in the extravesicular half of the RSR membrane profile, relative to the electron density level of the intravesicular and extravesicular aqueous spaces about $x = 0$ and $|x| = D/2$, respectively, which was accompanied by a continually decreased amplitude of the phospholipid headgroup maximum at the extravesicular surface of the membrane, as shown in Fig. 9.

Thus, close inspection of these various RSR membrane profiles indicates that the incorporation of Ca^{2+} pump protein into the SR lipid bilayer significantly perturbs the lipid bilayer profile from the extravesicular surface of the RSR membrane profile throughout the hydrocarbon core of the membrane up to the layer of lipid polar headgroups at the intravesicular surface of the membrane profile; the greater perturbations appear to be localized in the extravesicular half of the RSR membrane profile. These perturbations indicate that the Ca^{2+} pump protein extends in these RSR membrane profiles from the extravesicular surface of the membrane profile penetrating into the hydrocarbon core of the membrane at least to the layer of lipid polar headgroups at the intravesicular surface; a larger portion of the Ca^{2+} pump protein mass appears to be localized within the extravesicular half of the membrane profile. It is important to note that the Ca^{2+} pump protein molecules cannot protrude significantly from the layer of lipid polar headgroups at the extravesicular surface of these RSR membrane profiles into the extravesicular aqueous space, owing to the close proximity of the neighboring unit cells at $|x| = D/2$. Also, since lipid polar headgroups and protein have comparable average electron densities, the Ca^{2+} pump protein molecules could penetrate the lipid polar headgroup layer at the intravesicular membrane surface without necessarily perturbing the profile distribution of these headgroups; they cannot, however, protrude significantly from this surface into the intravesicular aqueous space because of the small extent of the intravesicular aqueous space in the unit cell profiles of these RSR membranes.

The rather strongly asymmetric profile of the RSR membrane indicates that the vectorial distribution of the Ca^{2+} pump protein molecules must be somewhat asymmetric in the RSR membrane profile. Hence, the Ca^{2+} pump protein must be preferentially incorporated into the extravesicular side of the SR lipid profile. This fact would additionally account for (*a*) the inequalities in the profile extents of the intravesicular vs. extravesicular water spaces in these RSR multilayers as determined by the neutron diffraction studies; (*b*) the asymmetric heavy-metal staining of these membranes, as observed in the electron microscopy studies (the layer of heavy-metal stain [electron-dense bands] at the intravesicular surface of these RSR membranes being significantly narrower than the layer of stain at the extravesicular surface, as shown in Fig. 5 *B* and *B1*, and (*c*) neutron diffraction studies with RSR reconstituted with a mixture of SR lipids and dioleoyl lecithin (DOL) deuterated at the 2 and the 9:10 positions which have shown that the time-average length of the labeled DOL lipid chains facing the extravesicular surface is considerably greater than that in pure DOL, with essentially no such

perturbation occurring for those DOL molecules facing the intravesicular surface of the lipid bilayer (33). The protein profile obtained from an analysis of this data was found to be highly asymmetric.

Comparison of the RSR and the Isolated LSR Profile Structures

We have previously reported the most probable electron density profile of isolated SR with a L/P ratio equal to 102.2, which is shown in Fig. 11 *C*. In addition, we have recently derived the most probable electron density profile for LSR using identical methods of data analysis for two multilayer water contents as shown in Fig. 11 *D*, *E*. The unit cell profile contained the membrane pair of the flattened LSR vesicle clearly revealing the inherent asymmetry of the isolated LSR membrane profile. As with SR the two electron-dense maxima within $0 \leq |x| \leq D/4$ are associated with the phospholipid headgroups of the lipid bilayer within the membrane profile whose separation is ~40 Å (the same headgroup separation is observed for purified

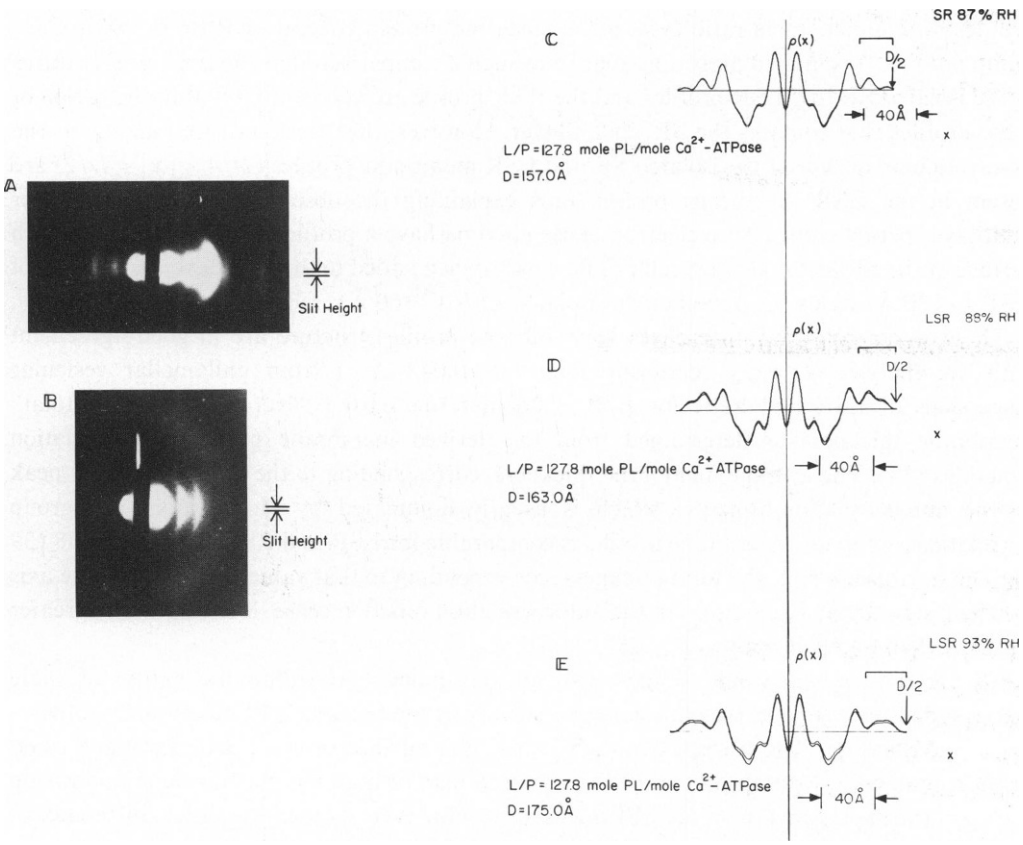

FIGURE 11 (*A*) Low-angle x-ray diffraction pattern of a partially dehydrated oriented multilayer of LSR membranes taken at 93% RH and 5°C. (*B*) High-angle pattern of the same specimen. (*C*) Most probable electron density profile of SR taken from Herbette et al. (14). (*D* and *E*) Most probable electron density profiles of LSR at 88 and 93% RH, respectively. The profile in (*E*) was calculated from the patterns shown in (*A* and *B*). The unit cell profile dimension, *D*, and the L/P mole ratio normalized to the amount of Ca^{2+} pump protein present in the membrane are indicated.

LSR lipid bilayers and for RSR membranes with L/P > 88). The asymmetry in amplitude and width of these two maxima associated with the phospholipid headgroups and the asymmetry evident in the hydrocarbon core of this membrane are presumed to be the result of perturbations of the LSR lipid bilayer induced by the presence of protein. The other main structural features of the LSR membrane profile are the two electron-dense maxima located at the extravesicular surface of the LSR membrane ($D/4 \leq |x| \leq D/2$), which are also likely to be associated with protein. The presence of protein in this region of the membrane profile is further substantiated by recent neutron diffraction studies which demonstrated that, although the profile extent of the extravesicular water space is considerably greater than that of the intravesicular water space, the water concentration in the extravesicular space is less than that of the intravesicular water space (27).

If the L/P mole ratios of SR and LSR are corrected with respect to the amount of Ca^{2+} pump protein present, we find that these corrected mole ratios for both are approximately 127.8 mole phospholipid/mol Ca^{2+} pump protein. Thus, we compare these profiles with RSR profiles at a similar mole ratio (Fig. 9 *D*), since the protein content of RSR is >95% Ca^{2+} pump protein. It is immediately apparent from such a comparison that the structural features of the isolated SR and LSR profiles and the RSR profile are very similar within the region of these profiles that contains the SR lipid bilayer. However, the electron dense maxima at the extravesicular surface of the isolated SR and LSR membrane profiles ($D/4 \leq |x| \leq D/2$) are absent in the RSR membrane profile, thus explaining the observed differences in their multilayer periodicities (these electron-dense maxima have a profile extent of ~20 Å at each surface of the SR and LSR unit cell profile which, when added to the multilayer periodicity of RSR (~120 Å) yields the periodicity of isolated LSR (~160 Å).

These similarities and differences in membrane profile structure are in good agreement with an analysis of x-ray scattering data ($s \leq 0.043$ Å^{-1}) from unilamellar vesicular dispersions of LSR and RSR for L/P > 88 in terms of the "average" and the "total" membrane thickness as determined from the derived membrane profile autocorrelation functions (34). The average membrane thickness, corresponding to the major nonorigin peak in the autocorrelation function which is usually dominated by phospholipid headgroup correlations across the membrane profile, is comparable for LSR and RSR with L/P > 88 (39 and 36 Å, respectively); the total thickness, corresponding to that value along the profile axis at which significant fluctuations in the autocorrelation function cease, is substantially greater for LSR than for RSR with L/P > 88.

The present results would suggest two obvious models regarding the nature of these electron-dense maxima at the extravesicular surface of the SR and LSR membrane profiles.

MODEL I The protein at the extravesicular surface of the LSR membrane could arise from non-Ca^{2+} pump protein (35–37), which may or may not play a role in optimizing the Ca^{2+} transport function of the LSR membrane. However, the weight-percent difference of Ca^{2+} pump protein in the RSR membrane vs. that in the LSR membrane is at most on the order of 10–20%; the presence of 10–20% non-Ca^{2+} pump protein is not likely to result in electron-dense maxima of such large amplitude at the extravesicular surface in the LSR membrane profile.

MODEL II The Ca^{2+} pump protein penetrates into the lipid bilayer to different degrees in LSR and RSR membranes with L/P > 88 such that a greater portion of the Ca^{2+}

pump protein protrudes from the extravesicular surface of the bilayer in isolated LSR. The remainder of the protein at the extravesicular surface may then arise from non-Ca^{2+} pump protein. This suggestion is reasonable since the molecular weight of the Ca^{2+} pump protein in both isolated and reconstituted SR is the same, thus eliminating the possibility that the absence of these electron dense features at the extravesicular surface of the RSR membrane profile is due to the loss of one or more nonessential subunits of the Ca^{2+} pump protein. We note that Model II is in agreement with several other studies (35, 38–41).

Conclusions

We have shown in the preceeding paper (1) that unilamellar reconstituted SR vesicles with L/P ratios comparable to LSR possessed 70–90% of the approximate initial Ca^{2+} transport rate and 60–70% of the efficiency of ATP-induced Ca^{2+} transport of isolated LSR controls. In this paper, for RSR membranes with L/P > 88, we have shown the following:

(*a*) The RSR membrane profile structure is highly asymmetric with a majority of the Ca^{2+} pump protein density occurring within the extravesicular half of the profile and a lesser portion of the protein spanning the lipid hydrocarbon core.

(*b*) The vectorial distribution of the Ca^{2+} pump protein in these RSR membrane profiles must therefore be asymmetric.

(*c*) These RSR membranes closely resemble the LSR membrane in profile structure within the region of the profile occupied by the lipid bilayer and Ca^{2+} pump protein. However, the LSR membrane profile contains features at its extravesicular surface which do not occur in the RSR membrane profile. These features, because of protein, arise only in part from non-Ca^{2+} pump protein in the LSR membrane.

(*d*) (*a–c*) above suggest that the majority of the Ca^{2+} pump protein, whose vectorial distribution in the RSR membrane profile is identical to that of LSR, may be more deeply embedded in the lipid bilayer of RSR, resulting in a lesser protrusion from the extravesicular surface of the bilayer than in LSR. This somewhat different positioning of the majority of the Ca^{2+} pump protein in the RSR and LSR membrane profiles may be due either to the absence of non-Ca^{2+} pump protein in RSR or to the minority of Ca^{2+} pump protein in RSR whose vectorial distribution is opposite to that of LSR.

(*e*) The somewhat lower estimated initial rates and efficiencies of RSR compared with LSR could arise from this less than optimal positioning of the majority of the Ca^{2+} pump protein in the RSR membrane profile and/or lack of total unidirectionality in the vectorial distribution of the pump protein in these RSR membranes. We are currently trying to quantify this latter point.

(*f*) In contrast to these RSR membranes with L/P > 88, RSR membranes with L/P < 88 possess dramatically different profile structures from those with L/P > 88 and LSR, which correlates with their dramatically diminishing Ca^{2+} transport capabilities with increasing protein content.

APPENDIX

This appendix serves to reveal the signficant difference in the profile structures of RSR membranes at low L/P ratio (in particular around L/P = 50–60) as compared to LSR and RSR with L/P > 88. The data in Fig. 4 clearly reveal that below a L/P ratio ≃88, the multilayer periodicity is significantly greater

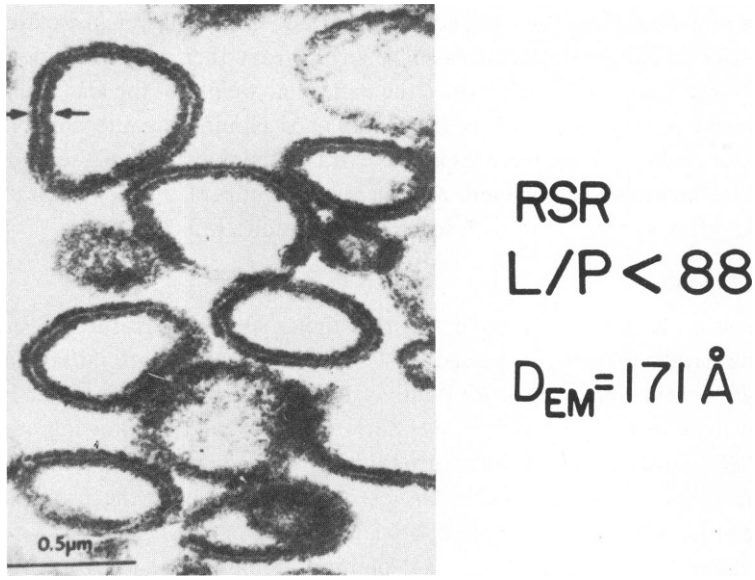

FIGURE A1 An electron micrograph of membraneous vesicles of RSR with L/P = 45.2. The arrows indicate the localization of heavy staining equally in both halves of the RSR membrane. The total membrane width averaged over several micrographs is equal to ~100 Å.

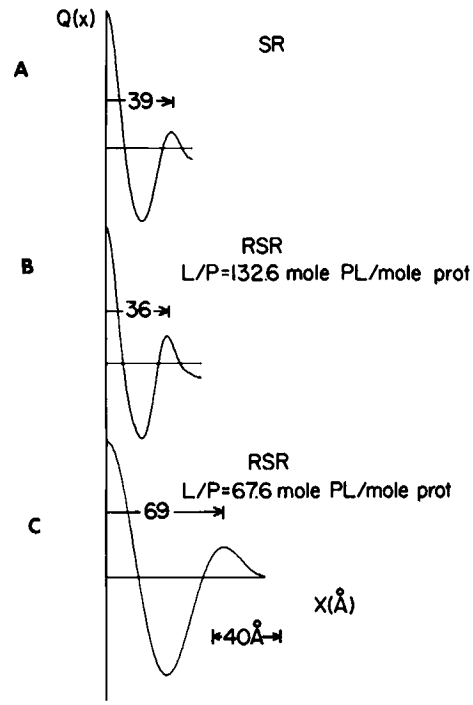

FIGURE A2 Membrane profile autocorrelation functions for (*A*) LSR, (*B*) RSR with L/P = 132.6, (*C*) RSR at a low L/P = 67.6. The solid line vectors correspond to the "average" membrane thickness: (see text for a description of the terms, average and total membrane thickness).

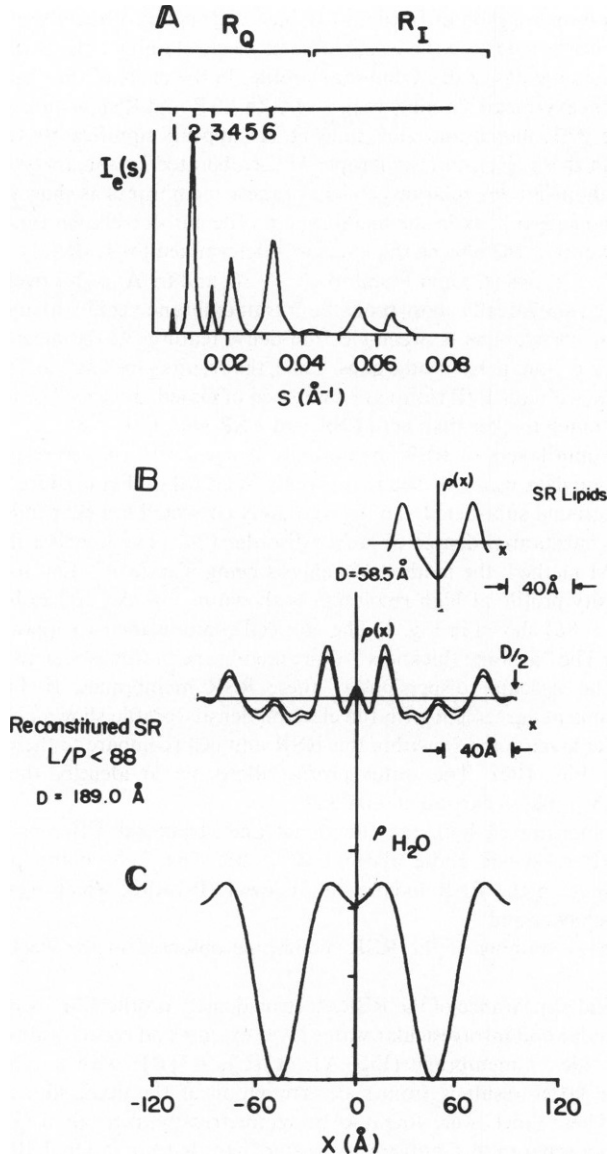

FIGURE A3 (*A*) Corrected experimental lamellar intensity function for an RSR multilayer with L/P = 41.5. (*B*) Electron density profile[2] of the RSR membrane multilayer determined from (*A*), truncated at $\pm D/2$ at 14 Å resolution. The unit cell of the multilayer again contains the membrane pair of the flattened RSR vesicle. The insert at top right shows the SR lipid bilayer profile for comparison. (*C*) The water profile of the RSR multilayer unit cell as determined by isomorphous H_2O/D_2O exchange. The absence of water around $|x| = 0.25D$ reflects the location of the lipid hydrocarbon core of the two RSR membranes in the unit cell which may be compared with the electron density profile shown in *B*.

compared with RSR > L/P = 88. Since we have most extensively studied RSR in the 50–60 L/P ratio range, evidence will be presented that clearly reveals that the RSR membrane at these low L/P ratios is much thicker and possesses a profile structure much different from both LSR and RSR with L/P > 88.

Fig. A1 is an electron micrograph of fixed and stained dispersions of membraneous vesicles of RSR with L/P = 45.2. The arrows indicate the localization of heavy staining equally on both surfaces of the RSR membrane for those regions of the membrane profiles in the plane of thin sectioning. This result is to be contrasted to the heavy-metal staining images of both LSR and RSR with L/P > 88 shown in Fig. 5 of the text. That the RSR membrane shown in Fig. A1 appears significantly thicker than LSR and RSR with L/P > 88 in these electron micrographs is corroborated by the analyses of x-ray scattering data obtained from unilamellar vesicular dispersions of these membranes as shown in Fig. A2. From the position of the major nonorigin peak in the membrane profile autocorrelation function calculated from these data (34) the "average" membrane thickness was determined for LSR (*A*), RSR with L/P > 88 (*B*) and RSR at low L/P ratios (*C*) and found to be 39, 36, and 69 Å, respectively. These dimensions, which correspond to the statistically most probable intramembrane vectors along the profile axis, are generally dominated by correlations between electron-dense features at the membrane surfaces across the membrane profile, e.g. lipid polar headgroups. Thus, the results presented in Figs. A1 and A2 reveal that dispersions of RSR with low L/P ratios are composed of closed, unilamellar, membraneous vesicles whose membranes are much thicker than both LSR and RSR with L/P > 88.

Hydrated, oriented multilayers of RSR membranes at low L/P ratios were likewise prepared and lamellar x-ray diffraction data was collected in a manner identical to that used for RSR with L/P > 88. Inspection of the background subtracted and appropriately corrected lamellar intensity function shown in Fig. A3, revealed a substantial degree of lattice disorder (24). The lamellar intensity function was phased by the GFSDM method, the method of analysis being identical to that used for SR. The most probable electron density profile at high resolution is shown in Fig. A3 (*B*) to be compared with the profiles of RSR (L/P > 88) shown in Fig. 9. The unit cell contains the two apposed membranes of the flattened RSR vesicle. The "average thickness" of the membrane profile is seen to be in agreement with that determined for the vesicular dispersions of these RSR membranes. In Fig. A3 (*C*) the low-resolution water profile is in agreement with the electron density profile shown above it with regards to the location of the water layer domains within this RSR unit cell (compare to the water profile for RSR [L/P > 88] shown in Fig. 10*c*). The water profile allows us to identify the center of the lipid hydrocarbon core in A3 (*B*) as occurring at ±0.25 *D*.

We have amply demonstrated both the functional and structural differences between the RSR membrane at low L/P ratio and those above L/P = 88. The Ca^{2+} pump protein may be more symmetrically distributed in the RSR membrane at low L/P ratios, which would account for their depressed functional behavior and

(*a*) symmetrical heavy staining of the RSR membrane observed in the electron microscope (Fig. A1).

(*b*) more symmetrical appearance of the RSR electron density profile (Fig. A3[*B*]).

(*c*) equal extravesicular and intravesicular water layer extents and concentrations (Fig. A3[C]).

(*d*) a significantly thicker membrane (Fig. A1, A2[*C*], A3[*B*]) with a symmetrically stretched hydrocarbon core (the latter result is from a determination of the deuterium label distributions by neutron diffraction). These labels were found to be symmetrically distributed about the center of the hydrocarbon core with a separation significantly greater than that found for RSR with L/P > 88. The electron dense maxima at $|x| = 17$ Å and $|x| = 77$ Å in Fig. A3(*B*) may arise from both protein and phospholipid headgroups resulting in an overall separation of 60 Å for these maxima in full agreement with the x-ray solution scattering results on vesicular dispersions of Fig. A2.

The authors would like to thank Miss Elaine Regan for preparation of the manuscript and Mrs. Mary Jo Larsen and Mr. Ken Ray for preparation of the figures.

This work was supported by grants from the National Institutes of Health HL 18708 to Drs. Blasie and Scarpa; AM 14632, Muscular Dystrophy Associations of America to Drs. Wang and Fleisher; and by a Cell and Molecular

Biology Institutional Training Grant Fellowship to Dr. Herbette. Dr. Scarpa is an Established Investigator of the American Heart Association.

Received for publication 22 October 1979 and in revised form 21 May 1981.

REFERENCES

1. Herbette, L., A. Scarpa, J. K. Blasie, D. Bauers, C. T. Wang, A. Saito, and S. Fleischer. 1981. Functional characteristics of reconstituted sarcoplasmic reticulum as a function of the lipid to protein ratio. *Biophys. J.* 36:27–46.
2. Wang, C. T., A. Saito, and S. Fleischer. 1979. Correlation of ultrastructure of reconstituted SR membranes with changes in lipid and protein composition. *J. Biol. Chem.* 254:9209–9219.
3. Lesslauer, W., and J. K. Blasie. 1971. X-ray holographic interferometry in the determination of planar multilayer structures. Theory and experimental observations. *Acta Crystallogr. A*27:456–461.
4. Cain, J., G. Santillan, and J. K. Blasie. 1972. Molecular motion as indicated by x-ray diffraction. *In* Membrane Research. C. F. Fox, editor. Academic Press, Inc., New York. 3–14.
5. Makowski, L., D. L. D. Caspar, W. C. Phillips, and D. A. Goodenough. 1977. Gap junction structures. II. Analysis of the x-ray diffraction data. *J. Cell Biol.* 74:629–645.
6. Blaurock, A. E. 1975. Bacteriorhodopsin: a transmembrane pump containing α-helix. *J. Mol. Biol.* 93:139–158.
7. Henderson, R. 1975. The structure of the purple membrane from halo-bacterium halobium: analysis of the x-ray diffraction pattern. *J. Mol. Biol.* 93:123–138.
8. Zaccai, G., J. K. Blasie, and B. P. Schoenborn. 1975. Neutron diffraction studies on the location of water in lecithin bilayer model membranes. *Proc. Natl. Acad. Sci. U.S.A.* 72:376–380.
9. Büldt, G., H. U. Gally, A. Seelig, J. Seelig, and G. Zaccai. 1978. Neutron diffraction studies on selectively deuterated phospholipid bilayers. *Nature (Lond.).* 271:182–184.
10. Pachence, J., L. Dutton, and J. K. Blasie. 1979. X-ray diffraction of reconstituted reaction center/lipid membranes. *Biochim. Biophys. Acta.* 548:348–373.
11. Hasselback, W., and L. G. Elfvin. 1967. Structural and chemical asymmetry of the calcium transporting membranes of the sarcotubular system as revealed by electron microscopy. *J. Ultrastruct. Res.* 17:598–622.
12. Deamer, D. W., and R. J. Baskin. 1969. Ultrastructure of sarcoplasmic reticulum preparations. *J. Cell Biol.* 42:296–307.
13. Saito, A., C. T. Wang, and S. Fleischer. 1978. Membrane asymmetry and enhanced ultrastructural detail of SR revealed with use of tannic acid. *J. Cell Biol.* 79:601–616.
14. Herbette, L., J. Marquardt, A. Scarpa, and J. K. Blasie. 1977. A direct analysis of lamellar x-ray diffraction from hydrated oriented multilayers of fully functional sarcoplasmic reticulum. *Biophys. J.* 20:245–272.
15. Lowry, O. H., N. J. Rosebrough, A. L. Farr, and R. J. Randall. 1951. Protein measurement with folin reagent. *J. Biol. Chem.* 193:265–275.
16. Meissner, G., and S. Fleischer. 1971. Characterization of sarcoplasmic reticulum from skeletal muscle. *Biochim. Biophys. Acta.* 241:356–378.
17. Meissner, G., G. E. Conner, and S. Fleischer. 1973. Isolation of sarcoplasmic reticulum by zonal centrifugation and purification of Ca^{2+}-pump and Ca^{2+} binding proteins. *Biochim. Biophys. Acta.* 298:246–269.
18. Meissner, G. 1975. Isolation and characterization of two types of sarcoplasmic reticulum vesicles. *Biochim. Biophys. Acta.* 389:51–68.
19. Santillan, G. G. 1976. An x-ray diffraction study: isolated retinal disk membranes. Ph.D. Thesis, University of Pennsylvania, Philadelphia, PA.
20. Schoenborn, B. P. 1977. Neutron protein crystallography. *TIBS* (September) 206–208.
21. Schoenborn, B. P., and A. C. Nunes. 1972. Neutron scattering. *Annu. Rev. Biophys. Bioeng.* 1:529–552.
22. Alberi, J., J. Fischer, U. Radeka, L. C. Rogers, and B. P. Schoenborn. 1975. A two-dimensional position-sensitive detector for thermal neutrons. *Trans. IEEE (Nuclear Science) NS*22:255–265.
23. Fleischer, S., B. Fleischer, and W. Stoeckenius. 1967. Fine structure of lipid depleted mitochondria. *J. Cell Biol.* 32:193–208.
24. Schwartz, S., J. E. Cain, E. A. Dratz, and J. K. Blasie. 1975. An analysis of lamellar x-ray diffraction from disordered membrane multilayers with application to data from retinal rod outer segments. *Biophys. J.* 15:1201–1233.
25. Kalina, M., and D. C. Pease. 1977. The preservation of ultrastructure in saturated phosphatidyl cholines by tannic acid in model systems and type II pneumocytes. *J. Cell Biol.* 74:726–741.

26. Kalina, M., and D. C. Pease. 1977. The probable role of phosphatidyl cholines in the tannic acid enhancement of cytomembrane electron contrast. *J. Cell Biol.* 74:742–746.
27. Herbette, L., A. Scarpa, B. P. Schoenborn, and J. K. Blasie. 1978. Analysis of lamellar neutron diffraction from functional SR. *Biophys. J.* 21:205*a*.
28. Engelman, D. M. 1971. Lipid bilayer structure in the membrane of *Mycoplasma laidlaivi*. *J. Mol. Biol.* 58:153–165.
29. Moody, M. F. 1963. X-ray diffraction pattern of nerve myelin! A method for determining the phases. *Science (Wash., D.C.)* 142:1173–1174.
30. Stamatoff, J. B., and S. Krimm. 1976. Phase determination of x-ray reflections for membrane-type systems with constant fluid density. *Biophys. J.* 16:503–516.
31. Levine, Y. K., and M. H. F. Wilkins. 1971. Structure of oriented lipid bilayers. *Nature (New Biol.)* 230:69–72.
32. Caspar, D. L. D., and W. C. Phillips. 1975. Dynamical effects in small-angle neutron diffraction from membranes. *Brookhaven Symp. Biol.* 27:(Section VII) 107–125.
33. Herbette, L., C. T. Wang, S. Fleischer, A. Scarpa, J. Seelig, and J. K. Blasie. 1979. Determination of the separate lipid and Ca^{2+} pump protein profile structure within reconstituted SR membranes via x-ray and neutron diffraction. *Biophys. J.* 25:90*a*.
34. Lesslauer, W., J. Cain, and J. K. Blasie. 1971. On the location of I-anilino-α-naphthalene-sulfonate in lipid model systems. *Biochem. Biophys. Acta.* 241:547–566.
35. Baskin, R. J., and D. W. Deamer. 1970. A membrane-bound creatine phosphokinase in fragmented sarcoplasmic reticulum. *J. Biol. Chem.* 245:1345–1347.
36. MacLennan, D. H. 1974. Isolation of proteins of the sarcoplasmic reticulum. *Methods Enzymol.* 32:291–302.
37. Ikemoto, N., J. Cucchiaro, and A. M. Garcia. 1976. A new glycoprotein factor of the sarcoplasmic reticulum. *J. Cell Biol.* 70:290*a*.
38. MacLennan, D. H., P. Seeman, G. H. Illes, and C. C. Yip. 1971. Membrane formation by the adenosine triphosphatase of sarcoplasmic reticulum. *J. Biol. Chem.* 246:2702–2710.
39. Inesi, G. 1972. Active transport of calcium ion in sarcoplasmic membranes. *Annu. Rev. Biophys. Bioeng.* 1:191–210.
40. Inesi, G., and D. Scales. 1974. Tryptic cleavage of SR protein. *Biochemistry.* 13:3298–3306.
41. Stewart, P. S., and D. H. MacLennan. 1974. Surface particles of sarcoplasmic reticulum membranes. *J. Biol. Chem.* 249:985–993.